JOURNAL OF THEORETICAL AND APPLIED MECHANICS
58, 4, pp. 927-941, Warsaw 2020
DOI: 10.15632/jtam-pl/124993

MODELING OF DYNAMIC GROWTH OF A MICRO-SCALED VOID BASED ON STRAIN GRADIENT ELASTO-PLASTICITY

Xinbing Ma

Jiangsu University, Faculty of Civil Engineering and Mechanics, Zhenjiang, Jiangsu Province, China

Jinxing Liu

Jiangsu University, Faculty of Civil Engineering and Mechanics, Zhenjiang, Jiangsu Province, China, and Wuhan University of Science and Technology, The State Key Laboratory of Refractories and Metallurgy, Wuhan, Hubei Province; e-mail: jxliu@mails.ucas.ac.cn

Jiadong Wang

Jiangsu University, Faculty of Civil Engineering and Mechanics, Zhenjiang, Jiangsu Province, China

Hao Pan

Institute of Applied Physics and Computational Mathematics, Beijing, China

Void initiation and growth serve as an important mechanism in ductile failures in metals. Particularly, on the micron-level, the extra hardening effect associated with strain gradient is accounted for by adopting strain gradient elasto-plasticity instead of the conventional plasticity. Effects of inertial, strain gradient hardening and thermal softening are formulated analytically for the case where a spherical void expands under external hydrostatic stress. As demonstrated by our results, the inertia effect firstly tends to hinder but then promotes the void growth. The threshold stress required for rapid void growth is lifted due to extra hardening of strain gradient so that the growth of a smaller void is delayed more remarkably. A considerable thermal softening phenomenon is observed here, which is caused by plastic work during the deformation process. The final void growth rate is mainly related to the maximum loading, which is consistent with the prediction based on the classical plastic theory.

Keywords: dynamic void growth, size effect, inertia, thermal softening

1. Introduction

As for high-quality ductile materials such as improved aluminum alloys and advanced high--strength steels, the research on their fracture and fatigue properties is becoming increasingly important. Benzerga and Leblond (2010) suggested that ductile fracture of metallic materials usually begins with void nucleation around external particles or other defects, then voids grow further when plastic deformation in the surrounding medium develops, and void coalescence finally leads to macro-level ductile fracture of the material.

Quasi-static void growth has been studied intensively. Huang *et al.* (1991) extended this research to elastic-plastic materials. Chung *et al.* (1987) investigated the cavity bifurcation of finite plastic materials under far-field hydrostatic tensile loads and found that cavitation stress was of the same order of magnitude as Young's modulus. Liu and Sayed (2013) studied the influence of the differences in void sizes on macro-level plastic deformations. Liu *et al.* (2014) analyzed the scale effect of void growth based on Taylor-plasticity. Notably, the tendencies under quasi-static loading can be dramatically different from the dynamic cases.

Studying dynamic void growth is necessary to understand void-based failures under fast--applied loadings such as impacts. Johnson (1981) studied void expansion in rate-dependent

viscoplastic solids. Ortiz and Molinari (1992) found that inertial effects dominated only when the void size was larger than the characteristic dimension. Cortés (1992) investigated the void growth of rigid plastic materials under hydrostatic and deviating stress by growth of voids. Wu *et al.* (2003a,b) concluded that the inertia effect first hindered and then promoted the growth of voids. Molinari and Wright (2005) suggested that in the early stages of void nucleation and growth, although thermal, viscoplastic and strain hardening effects matter, inertia was dominant. Navarro *et al.* (2018) experimentally observed that coalescence of voids could happen in the shear bands between matrix and inclusions in some alloy steels. Interestingly, in metallic glasses void defects also play a significant role in shear band nucleation (Luo *et al.*, 2018). Czarnota *et al.* (2006) proposed a model including inertia effect and matrix softening to simulate the whole dynamic growth of voids. Jacques *et al.* (2012) proposed a model to explain the dynamic effect caused by the growth of voids which hindered crack expansion. Sartori *et al.* (2015, 2016) emphasized the influence of void shape on strengths of porous ductile materials.

For micro-scale elastic-plastic deformation, there is a strong size effect in the yield strength, requiring a generalized plasticity. Fleck and Hutchinson (2001) proposed gradient theories (SGPs) to explain the size effect. Wu *et al.* (2003a) found that the gradient effect was able to increase the threshold stress required for voids growth, especially for smaller voids. Wilkerson and Ramesh (2014) examined the role of dislocation kinetics and substructure evolution on the dynamic growth of voids under very high strain rates. Although the size effect of voids has been well studied, the ability to capture the size effect of the elastic limit observed by Chakravarthy and Curtin (2011), Ehrler *et al.* (2008) and Liu *et al.* (2013) is yet available. On the micro-scale, the dominant mechanism behind the size effect is believed to be strain gradient effect instead of surface effect (Liu, 2015). Notably, in various versions of SGPs aforementioned, the size effect in the elastic limit (Ehrler *et al.*, 2008; Liu *et al.*, 2013), which has been proven experimentally to exist, is missing. To meet this challenge, Liu and Soh (2016) proposed a strain gradient elasto--plasticity (SGEP) that can capture all size effects, and we will analyze the gradient effect of the dynamic void growth based on SGEP.

In the high-rate deformation considerable amount of the plastic work will be converted into heat energy. Wright (2002) suggested that thermal softening plays a decisive role in the development of adiabatic shear bands during the high-rate deformation. In the unstable growth of voids, thermal softening of the material around the void may occur. The temperature of the void surface rises sharply and even reaches the melting point, so that the strength of the material is decreased. Thus, thermal softening weakens the gradient hardening, advancing voids growth. We will study the effects of inertia, temperature and gradient effects on the dynamic growth of voids.

This paper is organized as follows. Section 2 details the SGEP theoretical framework, introduces the temperature function and analyzes kinematics and equilibrium equations of the dynamic void growth. In Section 3, the effects of inertial, strain gradient hardening and thermal softening in dynamic void growth are studied and numerical simulations are discussed. Finally, a brief summary closes the paper in Section 4.

2. Theoretical formulation

2.1. Theoretical framework of SGEP

Here, both strains and strain gradients are expressed in an incremental form, where the strain increment is expressed as $\dot{\varepsilon}_{ij} = (\partial_i \dot{u}_j + \partial_j \dot{u}_i)/2$ and the strain gradient increment is expressed as $\dot{\eta}_{ijk} = \partial_{ij} \dot{u}_k$. The strain increment $\dot{\varepsilon}_{ij}$ is divided into a volume strain increment part $\dot{\varepsilon}_{kk}$ and a deviatoric strain increment part $\dot{\varepsilon}'_{ij}$. The strain gradient increment $\dot{\eta}_{ijk}$ has not been composed, resulting in introduction of only one plastic characteristic length l. The deviatoric

strain increment part $\dot{\varepsilon}'_{ij}$ and the strain gradient increment $\dot{\eta}_{ijk}$ are decomposed into an elastic and a plastic part, i.e.,

$$\dot{\varepsilon}'_{ij} = \dot{\varepsilon}'^{e}_{ij} + \dot{\varepsilon}^{p}_{ij} \qquad \dot{\eta}_{ijk} = \dot{\eta}^{e}_{ijk} + \dot{\eta}^{p}_{ijk} \tag{2.1}$$

The relation between stress and elastic strain is given as follows

$$\sigma_{ij} = \lambda \delta_{ij} \varepsilon^{e}_{mm} + 2\mu \varepsilon^{e}_{ij} \tag{2.2}$$

where σ_{ij} is the Cauchy stress, λ and μ are the Lamé constants. Here, according to the fact that the elastic scale parameters are much smaller than the plastic characteristic length, the elastic scale parameters are assumed to be zero and so that the higher order stresses are omitted.

Since only the plastic characteristic length is used, the total effective elastic-plastic strain $\varepsilon^{t,ep}_{e}$ can be written as

$$\varepsilon^{t,ep}_{e} = \left\{ (\varepsilon^{e}_{e} + \varepsilon_{e})^{2\beta} + [l(\eta^{e}_{e} + \eta_{e})]^{2\beta} \right\}^{\frac{1}{2\beta}} \tag{2.3}$$

where the contributions of strain and strain gradients to effective deformation and, therefore, plastic hardening are controlled by the parameter β.

The power hardening law is defined as

$$\sigma^{t} = \begin{cases} \sigma_Y + (\sigma^{t}_{0} - \sigma_Y) \dfrac{\varepsilon^{t,ep}_{e}}{\varepsilon^{t}_{0}} & \text{if} \quad \varepsilon^{t,ep}_{e} \leqslant \varepsilon^{t}_{0} \\ \sigma^{t}_{0} \Big(\dfrac{\varepsilon^{t,ep}_{e}}{\varepsilon^{t}_{0}} \Big)^{N} & \text{if} \quad \varepsilon^{t,ep}_{e} > \varepsilon^{t}_{0} \end{cases} \tag{2.4}$$

with

$$\varepsilon^{t}_{0} = \Big(\frac{\varepsilon^{t,ep}_{e}}{\varepsilon^{e}_{e} + \varepsilon_{e}} \Big)^{\gamma_\varepsilon} \varepsilon_Y \qquad \sigma^{t}_{0} = \Big(\frac{\varepsilon^{t,ep}_{e}}{\varepsilon^{e}_{e} + \varepsilon_{e}} \Big)^{\gamma_\sigma} \sigma_Y \tag{2.5}$$

where σ^{t} is the current yield strength, N is the hardening index, ε^{t}_{0} and σ^{t}_{0} are reference strain and stresses, respectively, γ_ε and γ_σ are material parameters to control how much ε^{t}_{0} and σ^{t}_{0} are altered by the gradient effect. We assume $\gamma_\sigma = 2\gamma_\varepsilon = 2\beta$ according to the flow rule proposed by Liu and Soh (2016).

2.2. Consideration of thermal softening

Most of the plastic work can be transformed into heat. Actually, such a phenomenon of thermal softening induced by plastic deformation is an important mechanism in the development of shear bands in metals under impact loadings. For classical plasticity, power law strain hardening with linear thermal softening is defined by Wu *et al.* (2003a)

$$\sigma = \sigma_Y f(\varepsilon) h(T^*) \tag{2.6}$$

where $f(\varepsilon)$ is the conventional yield function in terms of the effective strain, T^* is the temperature rise, and $h(T^*)$ is a function of the temperature rise.

In the present SGEP, we follow a similar manner to introduce the thermal softening effect. Then, the original yield criterion in Eq. (2.4) can be changed to

$$\sigma^{t} = \begin{cases} \sigma_Y + (\sigma^{t}_{0} - \sigma_Y) \Big(\dfrac{\varepsilon^{t,ep}_{e}}{\varepsilon^{t}_{0}} \Big) & \text{if} \quad \varepsilon^{t,ep}_{e} \leqslant \varepsilon^{t}_{0} \\ \sigma^{t}_{0} \Big(\dfrac{\varepsilon^{t,ep}_{e}}{\varepsilon^{t}_{0}} \Big)^{N} h(T^*) & \text{if} \quad \varepsilon^{t,ep}_{e} > \varepsilon^{t}_{0} \end{cases} \tag{2.7}$$

In Eq. (2.7), for $\varepsilon_e^{t,ep} > \varepsilon_0^t$ the material deforms in an elasto-plastic manner, considerable plastic strain causes softening. The temperature function in Eq. (2.7) is set as

$$h(T^*) = 1 - cT^* \tag{2.8}$$

where c is the coefficient of thermal softening, and is usually given in terms of the room temperature T_r and melting temperature T_m

$$c = \frac{1}{T_m - T_r} \tag{2.9}$$

We use the following relation between the temperature rise and plastic strain for an adiabatic deforming problem

$$\rho c_p dT = \widetilde{\eta}\sigma_e d\varepsilon^p \tag{2.10}$$

where ρ is metal density, c_p is specific heat, $\widetilde{\eta}$ defines percentage of plastic work transformed into heat, and it is set to 0.9 in this paper.

2.3. Dynamic growth of a void

In Fig. 1, assume that an infinite metal material containing a single void is subjected to the remote hydrostatic tensile stress p^{app}, and the material is assumed to be uniform and incompressible. The initial radius of the void is A, and the initial radius of a material point is R, as the hydrostatic tensile stress increases to a certain value, the void begins to grow, the current radius of the void is a, and the current radius of the reference point is r.

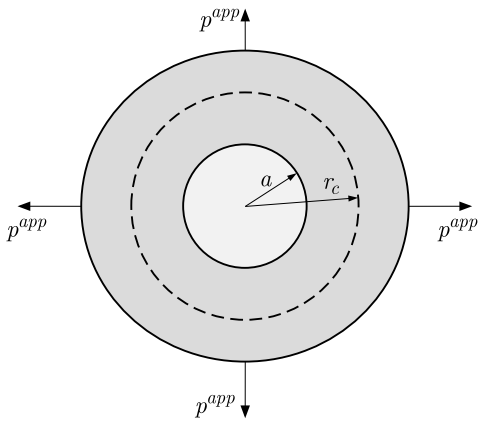

Fig. 1. A void growing in an infinite elasto-plastic medium under the remote hydrostatic tensile stress p^{app}. Yield starts from the void surface and propagates along the radius direction. The present radius of the void is a, the present interface between elastic and plastic region is noted by r_c

The incompressibility of the material results in the following relation,

$$r^3 - R^3 = a^3 - A^3 \tag{2.11}$$

By taking the derivative of time on both sides, we have

$$v_r = \dot{r} = \frac{a^2\dot{a}}{r^2} \tag{2.12}$$

The rate forms of strain and strain gradient components can be derived as

$$\begin{aligned}
&\dot{\varepsilon}_{rr} = \frac{dv_r}{dr} = -\frac{2a^2\dot{a}}{r^3} \qquad \dot{\varepsilon}_{\theta\theta} = \dot{\varepsilon}_{\varphi\varphi} = -\frac{1}{2}\dot{\varepsilon}_{rr} = \frac{a^2\dot{a}}{r^3} \\
&\dot{\eta}_{rrr} = \frac{\partial\dot{\varepsilon}_{rr}}{\partial r} = \frac{6a^2\dot{a}}{r^4} \qquad \dot{\eta}_{\theta\theta r} = \frac{\partial\dot{\varepsilon}_{\theta\theta}}{\partial r} = \frac{-3a^2\dot{a}}{r^4} \qquad \dot{\eta}_{\varphi\varphi r} = \frac{\partial\dot{\varepsilon}_{\varphi\varphi}}{\partial r} = \frac{-3a^2\dot{a}}{r^4} \\
&\dot{\eta}_{r\theta\theta} = \dot{\eta}_{\theta r\theta} = \frac{\dot{\varepsilon}_{rr} - \dot{\varepsilon}_{\theta\theta}}{r} = \frac{-3a^2\dot{a}}{r^4} \qquad \dot{\eta}_{r\varphi\varphi} = \dot{\eta}_{\varphi r\varphi} = \frac{\dot{\varepsilon}_{rr} - \dot{\varepsilon}_{\varphi\varphi}}{r} = \frac{-3a^2\dot{a}}{r^4}
\end{aligned} \tag{2.13}$$

In order to better distinguish the contributions made by the elastic part and the plastic part in the elasto-plastic deformation, we conduct the following elasto-plastic decomposition

$$\dot{a} = \dot{a}^e_\varepsilon + \dot{a}^p_\varepsilon \operatorname{sgn}(\dot{a}) = \dot{a}^e_\eta + \dot{a}^p_\eta \operatorname{sgn}(\dot{a}) \tag{2.14}$$

The strain and strain gradient components are decomposed into elastic and plastic parts

$$\dot{\varepsilon}_{ij} = \dot{\varepsilon}^e_{ij} + \dot{\varepsilon}^p_{ij} \qquad \dot{\eta}_{ijk} = \dot{\eta}^e_{ijk} + \dot{\eta}^e_{ijk} \tag{2.15}$$

The incremental forms of the elastic effective strain, plastic effective strain, elastic effective strain gradient and plastic effective strain gradient are, respectively

$$\dot{\varepsilon}^e_e = 2\frac{a^2\dot{a}^e_\varepsilon}{r^3} \qquad \dot{\varepsilon}_e = 2\frac{a^2\dot{a}^p_\varepsilon}{r^3} \qquad \dot{\eta}^e_e = 3\sqrt{\frac{5}{2}}\frac{a^2\dot{a}^e_\eta}{r^4} \qquad \dot{\eta}_e = 3\sqrt{\frac{5}{2}}\frac{a^2\dot{a}^p_\eta}{r^4} \tag{2.16}$$

The elastic strain can be obtained by integrating Eq. (2.16) in terms of time. Based on the elastic constitutive law, the stress component and effective stress can be obtained as follows

$$\begin{aligned} &\sigma_{rr} = 2\mu\varepsilon^e_{rr} \qquad \sigma_{\varphi\varphi} = 2\mu\varepsilon^e_{\varphi\varphi} \qquad \sigma_{\theta\theta} = 2\mu\varepsilon^e_{\theta\theta} \\ &\sigma_e = \sqrt{\frac{3}{2}\sigma'_{ij}\sigma'_{ij}} = 3\mu|\varepsilon^e_{rr}| = 6\mu\sum\frac{a^2\dot{a}^e}{r^3} \end{aligned} \tag{2.17}$$

The plastic strain can be obtained by integrating the incremental part of the plastic strain. From Eqs. (2.7)-(2.10), the plastic work done by plastic deformation and transformed heat energy can be obtained, and the effect of thermal softening can be accounted for.

According to Eq. (2.5), the reference strain and stress are, respectively

$$\varepsilon^t_0 = \varepsilon_Y\left[1 + \Big(\frac{3\sqrt{10}l}{4r}\Big)^{2\beta}\right]^{\frac{\gamma_\varepsilon}{2\beta}} \qquad \sigma^t_0 = \sigma_Y\left[1 + \Big(\frac{3\sqrt{10}l}{4r}\Big)^{2\beta}\right]^{\frac{\gamma_\sigma}{2\beta}} \tag{2.18}$$

The equation of motion for the above dynamic void growth can be written as

$$\frac{d\sigma_{rr}}{dr} - \frac{2\sigma_e}{r} = \rho\ddot{r} \tag{2.19}$$

The corresponding boundary condition is

$$\sigma(r,t) = 0 \quad \text{at} \quad r = a \qquad \sigma_r = p^{app} \quad \text{at} \quad r \to \infty \tag{2.20}$$

According to Eq. (2.11), the acceleration at the position r can be expressed in the form

$$\ddot{r} = -\frac{\partial}{\partial r}\Big(\frac{a^2\ddot{a}}{r} + \frac{2a\dot{a}^2}{r} - \frac{a^4\dot{a}^2}{2r^4}\Big) \tag{2.21}$$

By integrating Eqs. (2.19) and (2.21), the equilibrium equation can be obtained as

$$p^{app} - p^{res} = \rho\Big(a\ddot{a} + \frac{3\dot{a}^2}{2}\Big) \tag{2.22}$$

where, $\rho(a\ddot{a} + 3\dot{a}^2/2)$ represents the effect of inertia, and p^{res} is the resistant stress which can be expressed as

$$p^{res} = \int_a^\infty \frac{2\sigma_e}{r}\,dr = \int_{r_c}^\infty \frac{2\sigma_e}{r}\,dr + \int_a^{r_c}\frac{2\sigma_e}{r}\,dr = \frac{2}{3}\sigma^t_0\Big|_{r_c} + \int_a^{r_c}\frac{2\sigma_e}{r}\,dr \tag{2.23}$$

where $\sigma^t_0\Big|_{r_c}$ is the reference stress on the elastic-plastic boundary, which will become bigger than the traditional yield stress σ_Y due to the extra hardening effect associated with the strain gradient, resulting in a higher resistant stress.

3. Results and discussion

In all simulations, as shown in Fig. 2, the hydrostatic tensile load gradually increases from zero at a constant loading rate. At the moment t_1, the maximum loading p_s is reached. After that, the hydrostatic tensile load is kept constant as p_s for a timespan of t_2. We adopt material parameters determined by fitting corresponding experimental results for copper. Readers are referred to Liu and Soh (2016) for details.

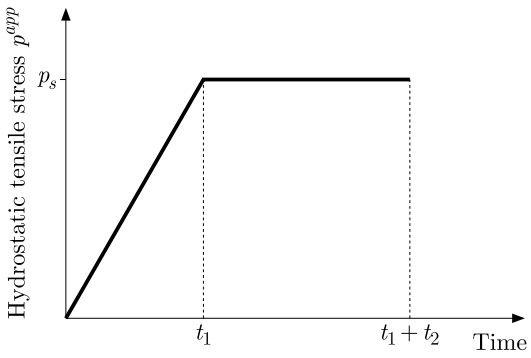

Fig. 2. The loading history of hydrostatic tensile stress applied externally

Table 1. Mechanical properties of the material according to Liu and Soh (2016)

Young's modulus	118 GPa	Yield stress	100 MPa
Poisson's ratio	0.35	Work-to-heat ratio	0.9
Specific heat	386 J/(kgK)	Density	$8.9 \cdot 10^3$ kg/m^3
Melting temperature	1358 K	T-softening coefficient	0.001 K^{-1}

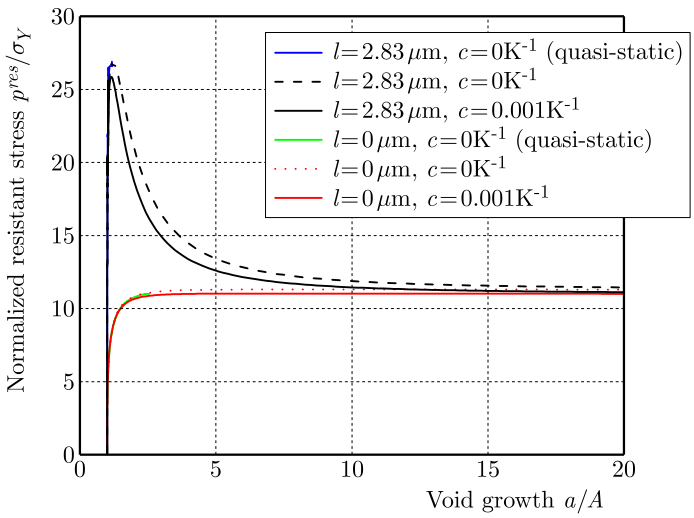

Fig. 3. The curves of the normalized resistant stress to relative growth of the void whose initial size is $A = 2\,\mu$m, with corresponding quasi-static results included. During the whole process the external applied stress p^{app} keeps increasing with a rate of 10 MPa/ns. Mechanical properties are shown in Table 1, dislocation coupling factor is $\beta = 0.5$ and $N = 0.22$

Figure 3 shows diagrams of normalized resistant stress versus void growth with and without the size effect or the thermal softening effect for a void with the initial radius $A = 2\,\mu$m. The mechanical properties of the material are shown in Table 1. Unless otherwise specified, the dislocation coupling factor $\beta = 0.5$ and hardening index $N = 0.22$ are adopted in this paper. It can be seen from Fig. 3 that for $l = 2.83\,\mu$m, as the void begins to grow, the resistant stress p^{res}

firstly increases quickly until it reaches a maximum value and then it begins to drop once the void growth a/A exceeds a critical value. The maximum value is defined as a "threshold stress" for unstable growth of the void and the critical value is typically less than 3. For the athermal condition, Wu *et al.* (2003a) obtained similar results. After the void growth exceeds the critical value, the resistance stress decreases and finally remains at a stable value for the unstable growth of the void consistent with the results predicted by classical plastic theory ($l = 0\,\mu$m). Thus, once the void expands to a certain degree, the medium around the void provides a constant resistance. For $l = 0\,\mu$m, the resistant stress p^{res} firstly increases quickly and then remains almost unchanged once it has reached a critical value. The quasi-static results are also included in Fig. 3 for comparison purposes. Since under quasi-static loading conditions, there is $p^{app} = p^{res}$, the void growth simultaneously stops once the applied stress does not increase any more. Thus in Fig. 3 we have only provided the increasing stages for quasi-static cases. Before the maximum loading has been reached, the void growth is stable, and only small deformation happens leading to unimportant influence of inertia. This explains why the quasi-static results get close to their athermal counterparts.

Whether l is zero or not, the adiabatic resistant stress ($c = 0.001\,\mathrm{K}^{-1}$) is lower than the athermal one ($c = 0\,\mathrm{K}^{-1}$). This is due to the fact that under the adiabatic condition, the plastic work is converted into heat energy at each material point, which will not be transferred elsewhere, resulting in a temperature rise at the very same material point. Thus, the elastic stiffness and the yield stress of the material point decreases due to thermal softening according to Eqs. (2.6) and (2.7). Such a thermal softening promotes void growth, and the material becomes more susceptible to damage. On the other hand, since thermal softening is neglected under the athermal conditions, the yield stress is relatively higher, the resistant value is relatively larger, and the void becomes more difficult to grow.

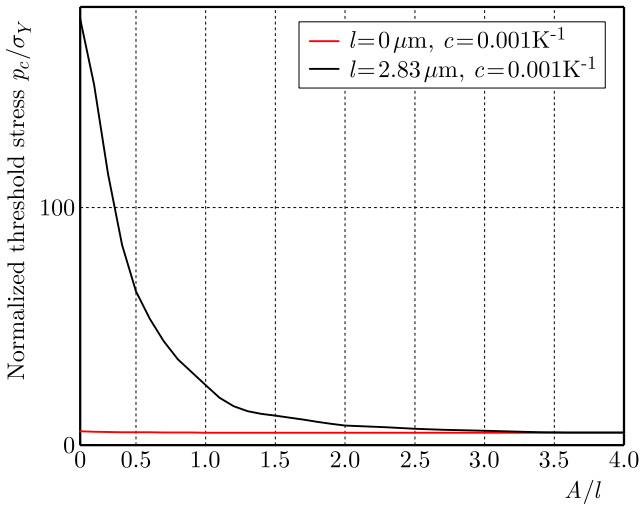

Fig. 4. The curves of normalized threshold stress, i.e. p_c/σ_Y versus the void radius normalized by the plastic characteristic length, i.e. A/l. The black solid line represents results with the gradient effect, and the red solid line without the gradient effect, for both of which thermal softening is accounted for. The material properties are shown in Table 1. The loading rate is 10 MPa/ns

When the gradient effect is considered by adopting $l = 2.83\,\mu$m, the threshold stress becomes higher with the decreasing initial radius of the void, as shown in Fig. 4. When the gradient effect is not considered, however, the threshold stress does not depend on the initial void size. As the initial void radius increases, the strain gradient and effective stress decrease sharply according to Eqs. (2.13)-(2.17) and, therefore, the gradient effect weakens quickly. When the initial radius is three times of the plastic characteristic length and above, the threshold stress gets close to the counterpart with no gradient effect, indicating feasibility of neglecting the gradient effect.

However, for a void size much smaller than it, the size dependence is so strong that neglecting the gradient effect would lead to a very inaccurate prediction.

Table 2 shows the material parameters used by Wu *et al.* (2003b) in studying dynamic void growth. The same parameters are used for simulating the voids with the initial radius being $A = 0.1\,\mu$m, $1\,\mu$m, $10\,\mu$m and $20\,\mu$m, respectively. As shown in Fig. 5, the hydrostatic tensile load increases at a rate of 0.1 GPa/ns for all cases. When neither the strain gradient effect nor thermal softening is accounted for, the present results, i.e. the black solid lines coincides well with those by Wu *et al.* (2003b), which serves as a validation of the present numerical procedure. When the load reaches roughly $3.6\sigma_Y$, the void begins to grow. Due to the inertia effect, the growth rate of the $A = 10\,\mu$m case is the slowest, and the $A = 0.1\,\mu$m case is the fastest. When the loading stops increasing, void growth continues under the drive of inertia. For the $A = 0.1\,\mu$m case, the growth rate starts to decrease once the external loading does not increase any more and, finally, the void expansion ceases. During the whole process, inertia will firstly hinders and then promotes the void growth.

Table 2. Mechanical properties of the material studied by Wu *et al.* (2003b)

Young's modulus	120 GPa	Yield stress	316.5 MPa
Poisson's ratio	0.361	Work-to-heat ratio	0.9
Specific heat	522 J/(kgK)	Density	$4.5 \cdot 10^3$ kg/m^3
Melting temperature	1941 ± 10 K	Softening coefficient	$5.206 \cdot 10^{-4}$ K^{-1}

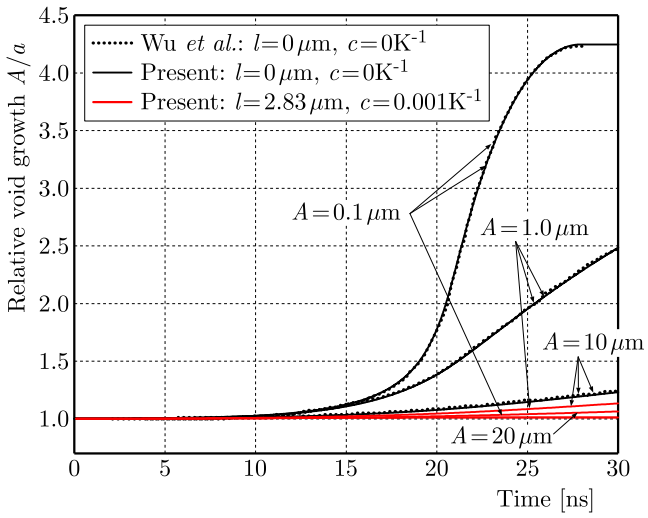

Fig. 5. The simulation results of dynamic growth of a void with the initial void size $A = 0.1\,\mu$m, $A = 1\,\mu$m, $A = 10\,\mu$m and $A = 20\,\mu$m, respectively, subjected to a prescribed loading with $p_s = 6.5\sigma_Y$. The dotted lines and the black lines represent the results of Wu *et al.* (2003b) and ours when the gradient effect is excluded, and the red solid lines are results by the present model when the gradient effect is considered. For all cases, the loading rate from 0 to t_1 is 0.1 GPa/ns

However, the above tendency is not valid any more if the effects of both strain gradient and thermal softening are included, as shown by red lines in Fig. 5, where for black dotted and solid lines, the athermal condition is adopted, while for red lines, the adiabatic condition is adopted. The material properties are listed in Table 2. The extra hardening effect due to strain gradient will lift the material strength and make the void growth harder to occur, but thermal softening tends to promote the growth. Namely, there is a competitive mechanism between these two influence factors. Particularly, when both effects are excluded the void of $A = 0.1\,\mu$m is the easiest one to grow, but it becomes the hardest one due to the strain gradient effect as indicated

by Eqs. (2.18) and (2.23). Under the influence of the gradient effect, the void has not started quick expansion for the loading of $p_s = 6.5\sigma_Y$. Moreover, the coordinate in Fig. 5 is the relative void growth, a/A instead of the present void size a itself, the line for $A = 10\,\mu$m is above that for $A = 20\,\mu$m.

In order to discuss the strain gradient effect in a separate manner, we temporarily exclude thermal softening and compare the results with and without the strain gradient effect. As shown in Fig. 6, four void sizes, i.e. $1\,\mu$m, $2\,\mu$m, $5\,\mu$m and $10\,\mu$m, are simulated. When the strain gradient is not considered, all voids with different initial radii begin to grow rapidly when the loading reaches $11\sigma_Y$. Under the action of inertia, the larger the initial radius, the slower the growth rate of the void, but eventually all the voids grow at the same speed, and the final growth rate is independent of the initial radius. When the strain gradient effect is included, the rapid void growth is delayed. The smaller the void, the more rapid growth is hindered. For example, for $A = 2\,\mu$m case, the void begins to grow rapidly as the loading reaches approximately $30\sigma_Y$, significantly higher than $11\sigma_Y$, the prediction without the strain gradient effect. For $A = 5\,\mu$m case, the starting time for rapid growth is delayed by 10 ns. After a long enough time, the void growth rate tends to be consistent with that without the strain gradient effect. For $A = 10\,\mu$m case, the strain gradient effect becomes so weak that two corresponding lines get close to each other. Particularly, for $A = 1\,\mu$m case, the final value of the external loading, i.e. $p_s = 35\sigma_Y$ is still much lower than the threshold stress for rapid void growth. In the above, extra hardening due to strain gradient increases the threshold stress required for rapid void growth, thus also delays the initiation of rapid growth. Such an influence is strongly dependent on the void size. A smaller void size corresponds to a stronger extra hardening due to the strain gradient.

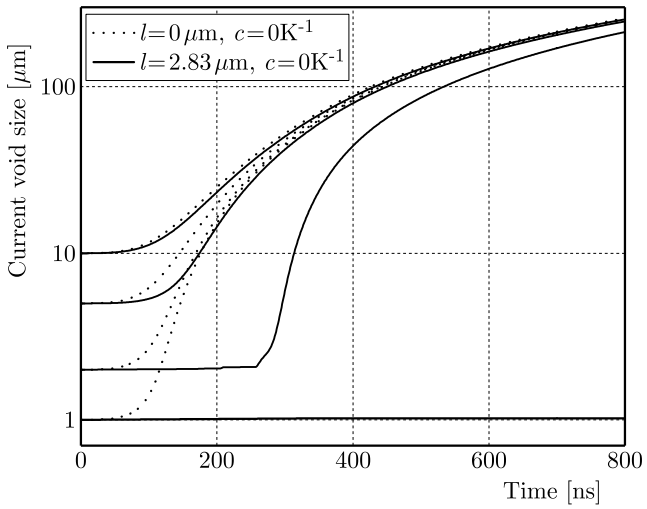

Fig. 6. Diagrams of current void size versus time with (solid) and without (dotted) the strain gradient effect showing the influence of the strain gradient. Thermal softening is excluded. Material parameters in Table 1 are used unless otherwise instructed. $p_s = 35\sigma_Y$, the loading rate is 10 MPa/ns

The radial distribution of yield strength is shown in Fig. 7, indicating an obvious size effect. In the present theory, the size dependence of yield strength is indeed allowed for, as shown in Eqs. (2.4) and (2.5). Generally speaking, more geometrically necessary dislocation (GND) is required around a smaller void. From Fig. 7, the reference strain on the void surface is $6.7\varepsilon_Y$ when $A = 1\,\mu$m, and $1.3\varepsilon_Y$ when $A = 2\,\mu$m, both of which are significantly higher than the conventional ε_Y. The reference strain is found to decrease sharply with the increasing normalized radial position. When the normalized distance is large enough, the reference strain gets closer to ε_Y. For $A = 10\,\mu$m, which is much larger than the plastic characteristic length $l = 2.83\,\mu$m, the above size effect becomes weaker and weaker.

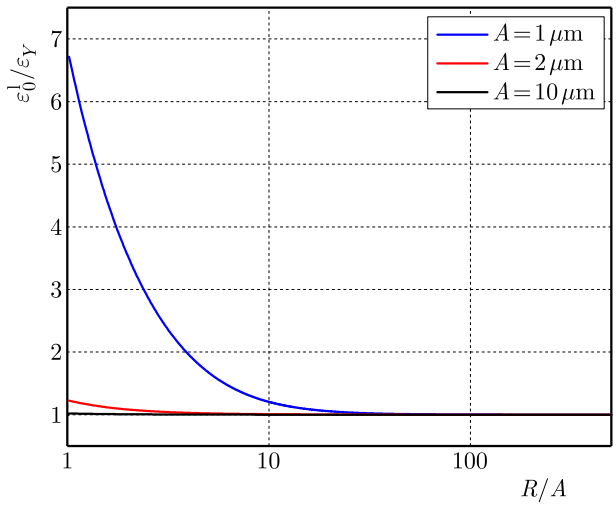

Fig. 7. The variation curves of the normalized reference strain versus radial distance from the void surface when the time is 150 ns which is smaller than t_1. Three initial void sizes are studied, i.e. $A = 1\,\mu$m, $2\,\mu$m and $10\,\mu$m, respectively. Mechanical properties of the material are shown in Table 1. The loading rate is 10 MPa/ns, the plastic characteristic length is $l = 2.83\,\mu$m, and the temperature effect is not considered by letting $c = 0\,\mathrm{K}^{-1}$

The size effect in the threshold stress for rapid void growth can also be seen in Fig. 8. When the gradient effect is excluded, the present theory reduces to the classical plasticity. From Fig. 8 it is seen that the threshold stress is independent of the initial void size. However, when the gradient effect is accounted for, the threshold stress increases quickly with the decreasing initial void size. For example, the void with $A = 1\,\mu$m has not begun growing rapidly even though the applied loading has reached $80\sigma_Y$.

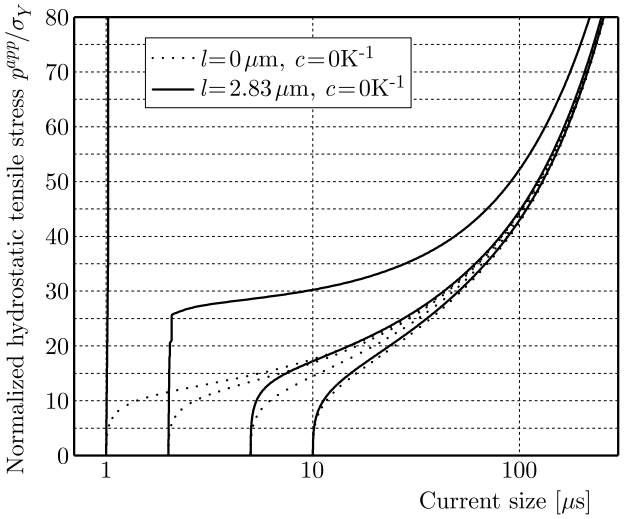

Fig. 8. Curves of the normalized hydrostatic tensile stress versus the current void size. The solid lines correspond to results with the gradient effect, and the dotted lines without the gradient effect. Material parameters in Table 1 are used unless otherwise instructed. The loading rate is 10 MPa/ns, $t_1 = 1000$ ns. Thermal softening is not considered

In order to study the influence of loading conditions on the dynamic void growth, we have provided results under four different loading rates, i.e. 0.05 GPa/ns, 0.01 GPa/ns, 0.005 GPa/ns and 0.001 GPa/ns, in Fig. 9, and results under four different maximum applied stresses, i.e. $p_s = 25\sigma_Y$, $30\sigma_Y$, $35\sigma_Y$ and $45\sigma_Y$, in Fig. 10. In Fig. 9, the time for initiation of rapid growth

varies with the prescribed loading rates. However, it is found that the void begins to grow when the loading reaches around $30\sigma_Y$ under all loading rates. In other words, the loading rate only has a negligible effect on the absolute value of the threshold stress for rapid growth. Nevertheless, under a lower loading rate, the rapid growth is initiated later. The red solid rectangles in Fig. 9 indicate the loading level of $31\sigma_Y$, although the loadings are consistent at different loading rates, the current sizes of the voids are greatly different. Besides, Fig. 10 shows that the maximum applied stress p_s plays a considerable role in the dynamic void growth. When $p_s = 25\sigma_Y$, rapid void growth is not possible to happen since the threshold stress has not been reached. For all p_s larger than $30\sigma_Y$, the void begins to grow rapidly at the same time. And a higher p_s results in a higher rate of rapid growth.

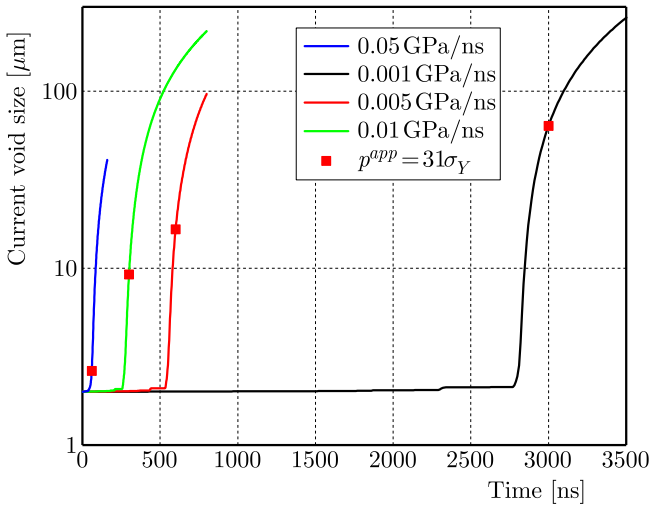

Fig. 9. Curves of the current void size versus time under the following loading rates: 0.05 GPa/ns, 0.01 GPa/ns, 0.005 GPa/ns, 0.001 GPa/ns, respectively. The mechanical properties of materials are shown in Table 1. The red solid rectangles indicate the current void size when the hydrostatic tensile load reaches $31\sigma_Y$. The plastic characteristic length is $l = 2.83\,\mu$m, the temperature effect is not considered

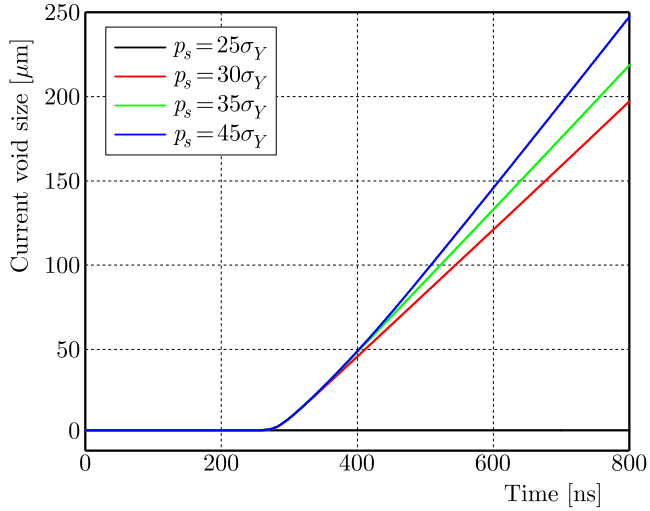

Fig. 10. Curves of the current void size versus time for four maximum hydrostatic tensile stresses, i.e. $p_s = 25\sigma_Y$, $30\sigma_Y$, $35\sigma_Y$, $45\sigma_Y$, respectively. The mechanical properties of materials are shown in Table 1. The loading rate is 0.01 GPa/ns, the plastic characteristic length is $l = 2.83\,\mu$m, and the temperature effect is not considered

Most of the plastic work done during plastic deformation will be converted into heat energy. Since the high loading rate adopted in this study, the heat exchange between each material point and its surroundings can be well neglected. As a result, the produced heat will cause the temperature of the very material point to rise, thus reducing the yield strength. Figure 11 shows the temperature rise around the void, the solid lines represent simulations considering the gradient effect, and the dotted lines represent simulations ignoring the gradient effect. It can be found that the temperature rise on the void surface is the highest, and the farther from the surface, the lower the temperature rise. With the gradient effect included, the temperature rise on the void surface exceeds 1000 K for $A = 1\,\mu$m, indicating possibility of melting. Even for the biggest void size $A = 10\,\mu$m, the induced temperature rise can still be as high as nearly 700 K. On the void surface, the temperature rise is obviously lifted by taking the gradient effect into account. However, this is not necessarily true throughout the studied domain. The gradient effect will enhance the elastic limit and, therefore, delays the occurrence of plastic initiation. Keep in mind that no heat is produced if the deformation is still purely elastic. This clearly explains why the gradient effect enlarges the temperature rise on the void surface, but reduces it in a certain radial distance range. In material points with a radial position large enough, it locates in the elastic deforming domain, thus the temperature rise is zero.

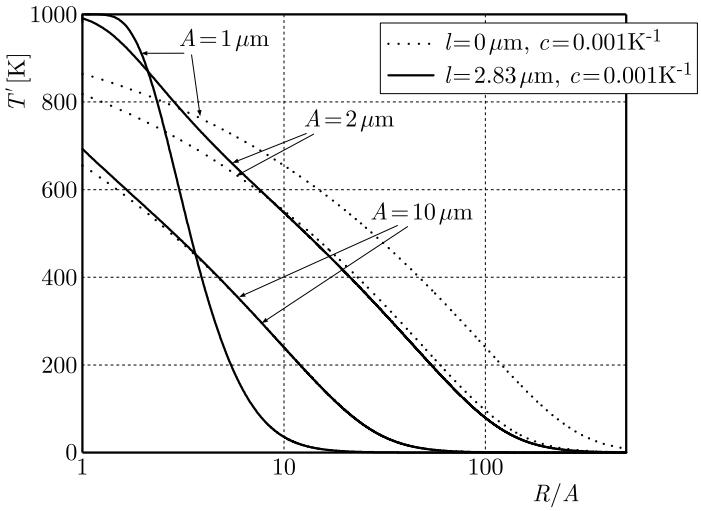

Fig. 11. Diagrams of temperature rise versus the radial position for void sizes $A = 1\,\mu$m, $A = 2\,\mu$m, $A = 10\,\mu$m, respectively. The solid and dotted lines are results with and without the gradient effect, respectively. The curves are drawn when the time is 150 ns from the beginning of applying the loading. The mechanical properties of the materials are shown in Table 1. The loading rate is 10 MPa/ns

Finally, with both the inertia and gradient effects included, we study the influence of thermal softening. Figure 12 shows results under both adiabatic and athermal conditions. For the biggest void size $A = 10\,\mu$m, the temperature effect affects the dynamic void growth very slightly. Considering the temperature effect, the void growth is brought forward by 4 ns for $A = 2\,\mu$m case, and even by 140 ns for $A = 1\,\mu$m case. When $A = 1\,\mu$m, the adiabatic threshold stress is $14\sigma_Y$ lower than the athermal one. Whether the temperature effect is accounted for or not, the void will not grow rapidly for $A = 0.8\,\mu$m case, mainly because the gradient effect is dominant now, which greatly increases the threshold stress required for rapid void growth. We firmly believe that there must exist a critical initial void radius in the range of $(0.8\,\mu\text{m}, 1\,\mu\text{m})$, when the void is able to rapidly grow under the adiabatic condition, but not able to grow under the athermal condition.

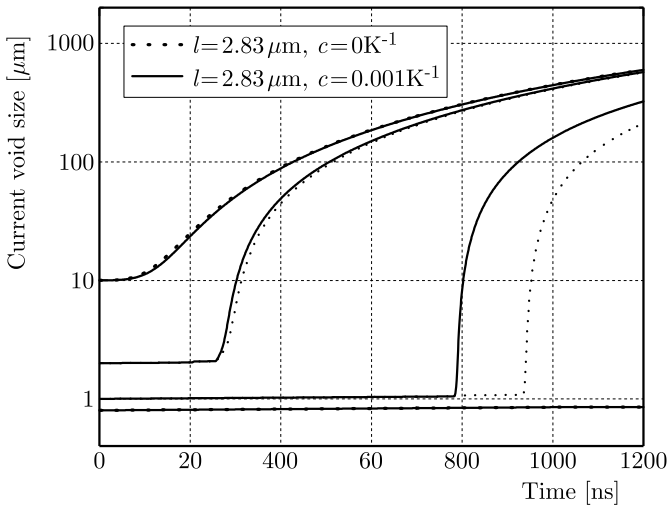

Fig. 12. The curves of current void size versus time for the following four initial void radii, i.e. $A = 0.8\,\mu$m, $1\,\mu$m, $2\,\mu$m and $10\,\mu$m, respectively. The solid and dotted lines are results with and without thermal softening, respectively. Material parameters in Table 1 are used unless otherwise instructed. The loading rate is 10 MPa/ns, the plastic characteristic length is $l = 2.83\,\mu$m. Both inertial and gradient effects are included

4. Conclusions

Based on the strain gradient elasto-plasticity recently proposed, we firstly reconstructed the yield function by considering thermal softening, the inertial effect and extra hardening effect due to strain gradient. Then the dynamic void growth problem is studied comprehensively.

In the early stage of void growth, inertia of material points around the void hinders the dynamic growth of the void, but then promotes it, and finally the growth rate gets close to the one predicted by the conventional plasticity. When the void size is of the order of $0.1\,\mu$m-$1\,\mu$m, the gradient effect greatly improves the yield stress in the neighborhood of the void. Meanwhile, the strain gradient elasto-plasticity can effectively capture the size effect of elastic limit, and the predicted elastic limit will be higher, so that the threshold stress of the void growth is also increased, resulting in a significant delay in time of the rapid void growth. Furthermore, most of the plastic work done at a material point is converted into heat energy, which causes the local temperature around the void surface to rise and even reach the melting point. The temperature rise weakens the yield strength of the material, reduces the threshold stress of the dynamic void growth, and thus promotes the dynamic void growth process.

Additionally, in this study, our focus is put on the spherical growth of voids. In some cases, the loading conditions can lead to significant deviations. Nevertheless, the present study still serves as an intuitive guide to a better understanding.

Acknowledgements

The work of J.X. Liu was supported by the State Key Laboratory of Refractories and Metallurgy (Wuhan University of Science and Technology). The work was supported by the National Science Foundation of China (Grant No. 11672119 and Grand No. 11972174).

References

1. Benzerga A.A., Leblond J.B., 2010, Ductile fracture by void growth to coalescence, *Advances in Applied Mechanics*, **44**, 169-305

2. Chakravarthy S., Curtin W.A., 2011, Stress-gradient plasticity, *Proceedings of the National Academy of Sciences*, **108**, 38, 15716-15720

3. Chung D., Horgan C., Abeyaratne R., 1987, A note on a bifurcation problem in finite plasticity related to void nucleation, *International Journal of Solids and Structures*, **23**, 7, 983-988

4. Cortés R., 1992, Dynamic growth of microvoids under combined hydrostatic and deviatoric stresses, *International Journal of Solids and Structures*, **29**, 13, 1637-1645

5. Czarnota C., Mercier S., Molinari A., 2006, Modelling of nucleation and void growth in dynamic pressure loading, application to spall test on tantalum, *International Journal of Fracture*, **141**, 1, 177-194

6. Ehrler B., Hou X.D., Zhu T.T., P'ng K.M.Y., Walker C.J., Bushby A.J., Dunstan D.J., 2008, Grain size and sample size interact to determine strength in a soft metal, *Philosophical Magazine*, **88**, 25, 3043-3050

7. Fleck N.A., Hutchinson J.W., 2001, A reformulation of strain gradient plasticity, *Journal of the Mechanics and Physics of Solids*, **49**, 10, 2245-2271

8. Huang Y., Hutchinson J., Tvergaard V., 1991, Cavitation instabilities in elastic-plastic solids, *Journal of the Mechanics and Physics of Solids*, **39**, 2, 223-241

9. Jacques N., Mercier S., Molinari A., 2012, Effects of microscale inertia on dynamic ductile crack growth, *Journal of the Mechanics and Physics of Solids*, **60**, 4, 665-690

10. Johnson J., 1981, Dynamic fracture and spallation in ductile solids, *Journal of Applied Physics*, **52**, 4, 2812-2825

11. Liu D., He Y., Dunstan D.J., Zhang B., Gan Z., Hu P., Ding H., 2013, Anomalous plasticity in the cyclic torsion of micron scale metallic wires, *Physical Review Letters*, **110**, 24, 244301

12. Liu J.X., 2015, Analysis of surface effects on the deformation of a nanovoid in an elasto-plastic material, *Applied Mathematical Modelling*, **39**, 17, 5091-5104

13. Liu J.X., Demiral M., El Sayed T., 2014, Taylor-plasticity-based analysis of length scale effects in void growth, *Modelling and Simulation in Materials Science and Engineering*, **22**, 7, 075005

14. Liu J.X., Soh A.K., 2016, Strain gradient elasto-plasticity with a new Taylor-based yield function, *Acta Mechanica*, **227**, 10, 3031-3048

15. Liu J.X., Sayed T.E., 2013, A variational constitutive model for the distribution and interactions of multi-sized voids, *International Journal of Damage Mechanics*, **23**, 1, 124-152

16. Luo Y., Yang G., Shao Y., Yao K., 2018, The effect of void defects on the shear band nucleation of metallic glasses, *Intermetallics*, **94**, 114-118

17. Molinari A., Wright T.W., 2005, A physical model for nucleation and early growth of voids in ductile materials under dynamic loading, *Journal of the Mechanics and Physics of Solids*, **53**, 7, 1476-1504

18. Navarro P.F., Chiu P.-H., Higgins A., Serge M., Benson D.J., Nesterenko V.F., 2018, Shear band patterning and post-critical behavior in AISI 4340 steel with different microstructure, *International Journal of Impact Engineering*, **112**, 144-154

19. Ortiz M., Molinari A., 1992, Effect of strain hardening and rate sensitivity on the dynamic growth of a void in a plastic material, *Journal of Applied Mechanics*, **59**, 1, 48

20. Sartori C., Mercier S., Jacques N., Molinari A., 2015, Constitutive behavior of porous ductile materials accounting for micro-inertia and void shape, *Mechanics of Materials*, **80**, 324-339

21. Sartori C., Mercier S., Jacques N., Molinari A., 2016, On the dynamic behavior of porous ductile solids containing spheroidal voids, *International Journal of Solids and Structures*, **97-98**, 150-167

22. Wilkerson J., Ramesh K., 2014, A dynamic void growth model governed by dislocation kinetics, *Journal of the Mechanics and Physics of Solids*, **70**, 262-280

23. Wright T., 2002, *The Physics and Mathematics of Adiabatic Shear Bands*, Cambridge University Press, Cambridge

24. Wu X.Y., Ramesh K.T., Wright T.W., 2003a, The coupled effects of plastic strain gradient and thermal softening on the dynamic growth of voids, *International Journal of Solids and Structures*, **40**, 24, 6633-6651

25. Wu X.Y., Ramesh K.T., Wright T.W., 2003b, The dynamic growth of a single void in a viscoplastic material under transient hydrostatic loading, *Journal of the Mechanics and Physics of Solids*, **51**, 1, 1-26

Manuscript received October 21, 2019; accepted for print February 25, 2020